Azo Anion Radical Complexes of Osmium and Related Nonradical Species

Kausikisankar Pramanik, Maya Shivakumar, Prasanta Ghosh, and Animesh Chakravorty*

Department of Inorganic Chemistry, Indian Association for the Cultivation of Science, Calcutta 700 032, India

Received July 14, 1999

The reaction of $[Os(H)(Br)(CO)(PPh_3)_3]$, **5**, with 2-(phenylazo)pyridine (pap) in boiling dry heptane has afforded the azo anion radical complex $[Os(pap^{\bullet-})(Br)(CO)(PPh_3)_2]$, **6a**, as the major product and $[Os(pap)(H)(CO)(PPh_3)_2]Br$, **7**, as a minor byproduct. Upon replacing pap by the better π-acceptor azo-2,2′-bipyridine (abp) in the above synthesis, the radical complex $[Os(abp^{\bullet-})(Br)(CO)(PPh_3)_2]$, **6b**, becomes the sole product. It is proposed that **6** is formed via homolytic cleavage of the Os−H bond in **5**; in the formation of **7**, the Os−Br bond of **5** is heterolytically cleaved. The X-ray structures of **6b** and **7**·CH_2Cl_2 have been determined. In **6b**, the N−N length is 1.35(2) Å, consistent with the anion radical description; in **7**·CH_2Cl_2 the length is 1.27(1) Å. The spin-bearing extended Hückel HOMO in a model of **6** is found to be ∼70% azo-π* in character associated with a small metal contribution. An electronic band observed in the range 600−700 nm in solutions of **6** is assigned to the HOMO → LUMO transition, the LUMO being 95% pyridine-π* in character. One-electron paramagnetic **6** displays well-defined anisotropic EPR features near $g = 2.00$. The anisotropy arises from the metal character of HOMO and is magnified by the large spin−orbit coupling in osmium. In a moisture-free environment **6** is indefinitely stable in the solid state, but in CH_2Cl_2−MeCN solution **6a** is rapidly oxidized by air, affording $[Os(pap)(Br)(CO)(PPh_3)_2]^+$, $\mathbf{6a}^+$, which has been isolated as the diamagnetic PF_6^- salt; $\mathbf{6b}^+PF_6^-$ has been similarly prepared. The voltammetric reduction potentials of the $\mathbf{6}^+/\mathbf{6}$ couple follow the order $\mathbf{6a}^+/\mathbf{6a} < \mathbf{6b}^+/\mathbf{6b}$, and the carbon monoxide stretching frequencies follow the order **6a** < **6b** and $\mathbf{6a}^+ < \mathbf{6b}^+$. These trends are consistent with the π-acidity order pap < abp. Crystal data are as follows: (**6b**, $C_{47}H_{38}BrN_4OOsP_2$) monoclinic, space group $P2_1/c$ (no. 14), $a = 10.215(4)$ Å, $b = 17.634(7)$ Å, $c = 22.473(8)$ Å, $\beta = 97.67(3)°$, $Z = 4$; (**7**·CH_2Cl_2, $C_{49}H_{42}BrCl_2N_3OOsP_2$) monoclinic, space group $P2_1/n$ (no. 14), $a = 15.323(7)$ Å, $b = 15.201(6)$ Å, $c = 19.542(7)$ Å, $\beta = 92.51(3)°$, $Z = 4$.

Introduction

The generally facile reduction of azo compounds in free[1,2] as well as coordinated[2−4] states is ensured by the low-lying nature of the azo-π* orbital. One-electron reduction, eq 1,

$$-N{=}N- + e \rightarrow -N^{\cdot\cdot\cdot}N- \qquad (1)$$

generates an azo anion radical. Though observable in solution,[1−4] such radicals have generally eluded isolation in pure form. The situation has just begun to change with the characterization of a few crystalline ruthenium[5,6] and copper[7] chelates.

In the present work we explore the case of osmium using azopyridines as reducible ligands. A synthetic strategy has been developed and successfully applied for isolation of the title complexes. Bond parametric, spectroscopic, and molecular orbital findings are found to converge to a predominant azo anion radical description of the species. Nonradical congeners formed via one-electron electrochemical/chemical oxidation have been isolated and characterized. The structure and properties of a hydrido byproduct that throws light on the nature of the radical-forming reaction are scrutinized.

Results and Discussion

Synthetic Studies. The two azo ligands (general abbreviation L) used in the present work are 2-(phenylazo)pyridine (pap) and azo-2,2′-bipyridine (abp). The binding of pap and its substituted derivatives to bivalent osmium in the form of the Os(L) chelate ring, **3**, is well-documented.[8−10] No Os(abp) complexes are however known. The Os(pap) type species are invariably electroactive[9] in solution and undergo one-electron reduction, presumably forming the anion radical entity $Os(L^{\bullet-})$, represented by the approximate valence bond structure **4**. However, all attempts to isolate such reduced species have failed.

This has prompted us to search for a qualitatively different synthetic strategy that can bypass preisolation of Os(L) species.

(1) (a) Sadler, J. L.; Bard, A. J. *J. Am. Chem. Soc.* **1968**, *90*, 1979. (b) Jonson, C. J.; Chang, R. *J. Chem. Phys.* **1965**, *43*, 3183.
(2) Goswami, S.; Mukherjee, R.; Chakravorty, A. *Inorg. Chem.* **1983**, *22*, 2825.
(3) (a) Pal, C. K.; Chattopadhyay, S.; Sinha, C. R.; Chakravorty, A. *Inorg. Chem.* **1994**, *33*, 6140. (b) Pal, C. K.; Chattopadhyay, S.; Sinha, C. R.; Chakravorty, A. *Inorg. Chem.* **1996**, *35*, 2442.
(4) Krause, R. A.; Krause, K. *Inorg. Chem.* **1984**, *23*, 2195. (b) Krejčík, M.; Záliš, S.; Klíma, J.; Sýkora, D.; Matheis, W.; Klein, A.; Kaim, W. *Inorg. Chem.* **1993**, *32*, 3362.
(5) Shivakumar, M.; Pramanik, K.; Ghosh, P.; Chakravorty, A. *Inorg. Chem.* **1998**, *37*, 5968.
(6) Shivakumar, M.; Pramanik, K.; Ghosh, P.; Chakravorty, A. *J. Chem. Soc., Chem. Commun.* **1998**, 2103.
(7) (a) Schwach, M.; Hausen, H.-D.; Kaim, W. *Inorg. Chem.* **1999**, *38*, 2242. (b) Doslik, N.; Sixt, T.; Kaim, W. *Angew. Chem.* **1998**, *110*, 2125; *Angew. Chem., Int. Ed. Engl.* **1998**, *37*, 2403.
(8) Ghosh, B. K.; Goswami, S.; Chakravorty, A. *Inorg. Chem.* **1983**, *22*, 3358.
(9) Ghosh, B. K.; Mukhopadhyay, A.; Goswami, S.; Chakravorty, A. *Inorg. Chem.* **1984**, *23*, 4633.
(10) (a) Mallick, T. K.; Roy, B. K.; Das, P. K.; Ghosh, B. K. *Transition Met. Chem.* **1993**, *18*, 609. (b) Mallick, T. K.; Roy, B. K.; Das, P. K.; Ghosh, B. K. *Indian J. Chem.* **1993**, *32A*, 580. (c) Mallick, T. K.; Roy, B. K.; Das, P. K.; Ghosh, B. K. *Polyhedron* **1994**, *13*, 1817. (d) Sinha, S.; Banerjee, A. K.; Ghosh, B. K. *Transition Met. Chem.* **1992**, *17*, 22.

10.1021/ic9908322 CCC: $19.00
Published on Web 12/28/1999

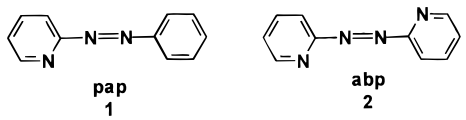

pap
1

abp
2

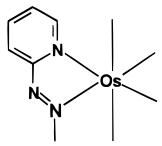

Os(L)
3

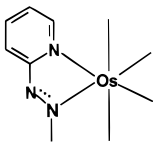

Os(L$^{\bullet-}$)
4

We looked for a starting material in which the obligatory reducing equivalent as well as certain radical-stabilizing features are already built-in. It was hoped that such a material would react with L, forming Os(L$^{\bullet-}$) directly. The experience with radical complexes of ruthenium[5,6] suggested the use of hydridic starting materials. The hydride **5**[11] was indeed found to ideally suit our design strategy.

[Os(H)(Br)(CO) $(PPh_3)_3$]
5

The reaction of **5** with excess pap (for abp, see below) in dry boiling heptane under nitrogen afforded the desired radical complex, green-colored **6a**, as the major product. Interestingly the similarly constituted but nonradical hydrido complex **7** was

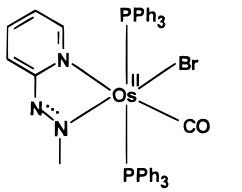

[Os(L$^{\bullet-}$)(Br)(CO)$(PPh_3)_2$]
6a, L$^{\bullet-}$ = pap$^{\bullet-}$
6b, L$^{\bullet-}$ = abp$^{\bullet-}$

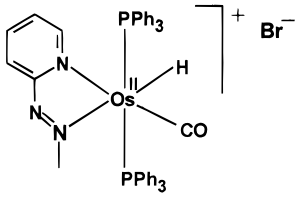

[Os(pap)(H)(CO)$(PPh_3)_2$]Br
7

obtained as a minor (~10%) byproduct. The choice of a dry hydrocarbon (here heptane) as the reaction solvent is crucial for the synthesis of the radical product. In polar solvents there is a strong tendency to form nonradical products.

The contrast between the reactions leading to **6a** and **7** is highlighted in eq 2 where only the relevant ligands of **5**, **6a**, and **7** are shown. It is logical to assume that in both cases the

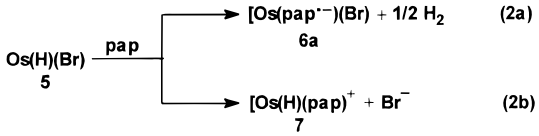

pap ligand first attaches itself to the metal site of **5** by displacing a labile PPh_3 ligand. In the route to **6a** (eq 2a), *homolytic* cleavage of the Os−H bond occurs. This provides the electron required for in situ pap$^{\bullet-}$ formation, and the vacated site is utilized to complete pap$^{\bullet-}$ chelation. In eq 2b the Os−Br bond is cleaved *heterolytically*, and chelation by pap is completed, affording **7**. The relative yields of the two products show that the path of eq 2a is much more facile than that of eq 2b.

An increase in the π-acidity of the azo ligand should favor the route of eq 2a even further. This indeed happens upon replacing pap by abp in the above synthetic procedure. Here the abp$^{\bullet-}$ anion radical complex, **6b**, is the sole product (π-acidity: abp > pap). Facile homolytic M−H cleavage also favors radical formation. Thus, the reaction of hydridic ruthenium starting materials with L furnishes only Ru(L$^{\bullet-}$) species[5,6] (ease of M−H cleavage: Ru > Os).

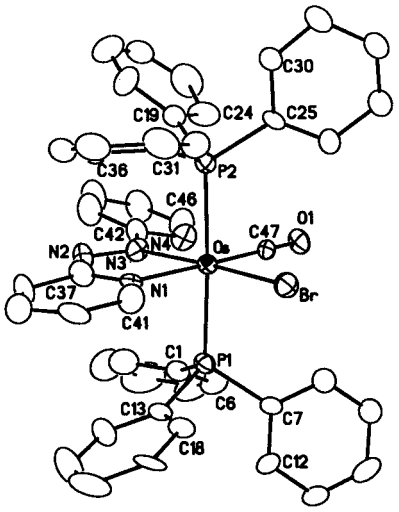

Figure 1. Molecular structure of [Os(abp$^{\bullet-}$)(Br)(CO)$(PPh_3)_2$] (**6b**) showing 30% probability ellipsoids.

In a moisture-free environment the type **6** complexes are indefinitely (more than two years) stable in the solid state. However, upon stirring CH_2Cl_2−MeCN solutions containing **6** and NH_4PF_6 in air, rapid aerial oxidation to **6**$^+$ occurs. The latter

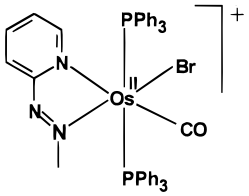

[Os(L)(Br)(CO)$(PPh_3)_2$]$^+$
6a$^+$, L = pap
6b$^+$, L = abp

has been isolated as dark-colored **6**$^+PF_6^-$ salts. The detailed structure of **6**$^+$ could not be determined due to a lack of single crystals. The structures of ruthenium analogues are, however, known.[5,12]

Physical data of the complexes synthesized in this work are partly set out in the tables, and the remaining information is incorporated in the Experimental Section.

Structure. The X-ray structure of **6b** has been determined. A molecular view is shown in Figure 1, and selected bond parameters are listed in Table 1. The coordinated azo and pyridine nitrogen atoms of the chelated abp$^{\bullet-}$ ligand lie trans to Br$^-$ and CO, respectively, in the distorted octahedral coordination sphere. The chelate ring is coplanar with the coordinated pyridine ring, and the pendant pyridyl ring makes a dihedral angle of 20.0° with it.

In uncoordinated azo compounds and hydrazines the N−N distances are 1.25 Å[13] and 1.45 Å,[14] respectively. In **6b**, the

(11) Ahmad, N.; Levason, J. J.; Robinson, S. D.; Utterley, M. F. *Inorg. Synth.* **1975**, *15*, 45.
(12) The X-ray structure of [Ru(abp)Cl(CO)$(PPh_3)_2$]PF_6 has been determined, and the details will be reported elsewhere.

Table 1. Selected Bond Distances (Å) and Angles (deg) and Their Estimated Standard Deviations for 6b and 7·CH_2Cl_2

	6b	**7**·CH_2Cl_2		**6b**	**7**·CH_2Cl_2
Os−P1	2.395(5)	2.382(3)	Os−N3	2.044(15)	2.095(10)
Os−P2	2.389(5)	2.377(3)	Os−C47/C48[a]	1.914(22)	1.842(13)
Os−Br	2.584(2)		N2−N3	1.348(22)	1.274(13)
Os−N1	2.172(16)	2.118(10)			
P1−Os−P2	176.5(2)	163.1(1)	P1−Os−N3	89.8(5)	97.7(3)
N1−Os−C47/C48[a]	176.0(7)	174.5(5)	P1−Os−Br	91.9(1)	
N3−Os−Br	167.7(5)		P1−Os−C47/C48[a]	91.6(6)	89.2(4)
N1−Os−N3	75.5(7)	73.8(4)	P2−Os−N1	88.6(4)	93.2(3)
N1−Os−Br	92.4(5)		P2−Os−N3	89.2(5)	99.2(3)
N3−Os−C47/C48[a]	100.5(7)	100.7(5)	P2−Os−Br	88.4(1)	
Br−Os−C47/C48[a]	91.6(5)		P2−Os−C47/C48[a]	91.9(6)	87.9(4)
P1−Os−N1	87.9(4)	91.3(3)			

[a] C47 in **6b** and C48 in **7**·CH_2Cl_2.

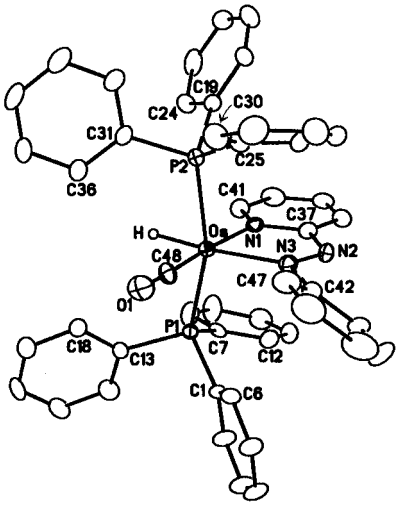

Figure 2. Molecular structure of the cation $[Os(pap)(H)(CO)(PPh_3)_2]^+$ in the crystal of **7**·CH_2Cl_2 showing 30% probability ellipsoids.

distance is of intermediate value, 1.35(2) Å. This is qualitatively consistent with an anion radical description of the azo ligand in the complex. In going from −N═N− ($\sigma^2\pi^2$) to −N⋯N− ($\sigma^2\pi^2\pi^{*1}$), the bond order decreases from 2 to 1.5; in hydrazines the bond order is 1. We note that in the reported ruthenium anion radical species the average N−N length is also 1.35 Å.[5,6] The observed Os−P, Os−Br, and Os−CO lengths are more or less unexceptional.[15−17]

The structure of the solvate **7**·CH_2Cl_2 has also been determined (Figure 2, Table 1). The gross coordination geometry is the same as in **6b** but with replacement of Br^- by H^- and $abp^{\bullet-}$ by pap. Here, unlike in **6b**, the P(1)OsP(2) axis deviates considerably (∼17°) from linearity. The pendant phenyl ring makes a dihedral angle of 35.7° with the plane of the chelate ring. The Os−N(azo) length is longer in **7**·CH_2Cl_2 than in **6b**, presumably due to the strong trans influence of the hydride ligand.

The hydride ligand is not observable in difference Fourier maps, although its presence is indirectly reflected in the other structural features noted above such as pronounced P(1)OsP(2) nonlinearity and Os−N(azo) lengthening. In ^{1}H NMR of **7** the hydride resonance occurs at −9.13 ppm as a well-resolved triplet corresponding to coupling with two equivalent ^{31}P nuclei (J = 22.5 Hz).

Frontier Orbitals, Magnetism, and Spectra. To gain insight into the approximate composition of the frontier orbitals in type **6** complexes, extended Hückel calculations were performed on a simplified model (Ph/C_5H_4N groups replaced by H). The half-filled HOMO, depicted in **8**, is indeed primarily azo-π^* in character (70%) but with significant pyridyl-π^* (15%) and metal-d_{yz} (10%) contributions. The ligands not shown in **8** have little or no contributions. The LUMO, **9**, lying ∼2 eV above **8**

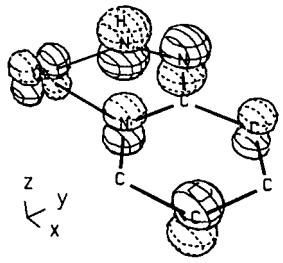

8

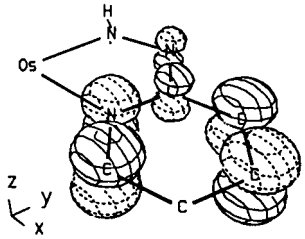

9

is a nearly pure (95%) pyridyl-π^* orbital. The metal-t_2 orbitals have some Br^- character and lie below **8**. In going from **6** to $\mathbf{6}^+$, the orbital **8** becomes the LUMO and the HOMO is primarily metal-t_2 in nature.

The room-temperature magnetic moments of the polycrystalline complexes (**6a,** 1.96 μ_B; **6b,** 1.94 μ_B) correspond to the presence of one unpaired electron (S = 1/2). The same samples display well-defined EPR features near g = 2 (**6a**, 1.998, 1.966; **6b,** 2.001, 1.971). The spectra are approximately axial, with the perpendicular resonance showing some signs of rhombic splitting (Figure 3). The small anisotropy, unresolved in the analogous ruthenium species,[5,6] is consistent with the presence

(13) (a) Mostad, A.; Rømming, C. *Acta Chim. Scand.* **1971**, *25*, 3361. (b) Chang, C. H.; Porter, R. F.; Brauer, S. H. *J. Am. Chem. Soc.* **1970**, *92*, 5313. (c) Roy, T.; Sengupta, S. P. *Cryst. Struct. Commun.* **1980**, *9*, 965.
(14) Morino, Y. Iijima, T.; Murata, Y. *Bull. Chem. Soc. Jpn.* **1960**, *33*, 46.
(15) (a) Ghosh, P.; Bag, N.; Chakravorty, A. *Organometallics* **1996**, *15*, 3042. (b) Pramanik, K.; Ghosh, P.; Chakravorty, A. *J. Chem. Soc., Dalton Trans.* **1997**, 3553.
(16) (a) Fergusson, J. E.; Robinson, W. T.; Coll, R. K. *Inorg. Chim. Acta* **1991**, *181*, 79. (b) Robinson, P. D.; Ali, I. A.; Hinckley, C. C. *Acta Crystallogr.* **1991**, *C47*, 1397.
(17) (a) Bottomley, F.; Ivan, J. B.; Peter, L.; White, S. *J. Chem. Soc., Dalton Trans.* **1978**, 1726. (b) Clark, G. R.; Collins, T. J.; Marsden, K.; Roper, W. R. *J. Organomet. Chem.* **1978**, *157*, C23.

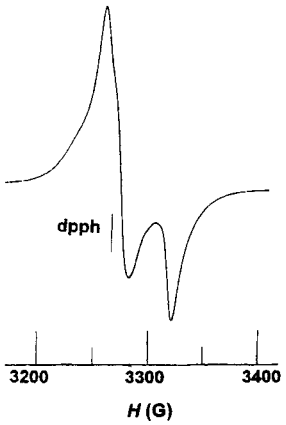

Figure 3. Powder EPR spectrum of **6b** in the X-band (9.1 GHz) at 298 K. Instrument settings: power, 30 dB; modulation, 100 kHz; sweep center, 3300 G; sweep width, 500 G; sweep time, 240 s.

of the small metal contribution to the spin-bearing HOMO, **8**. The amplification of the anisotropy in the osmium complexes is largely a spin−orbit phenomenon (coupling constant: Os ≫ Ru) which has been observed in other systems, e.g., in radical complexes of the nickel triad.[18] The lack of nitrogen hyperfine structure in the spectra of **6** is not unusual since the ^{14}N coupling constant in azo-π^* radicals is small and difficult to observe.[1b,3] The $\mathbf{6}^+$ species are diamagnetic and display well-resolved ^1H NMR spectra.

The electronic spectral band of **6** in the 600−700 nm region is assigned to the HOMO (**8**) → LUMO (**9**) transition. It is essentially an intraligand excitation of the anion radical electron from the azo to the pyridyl function. The band near 500 nm in $\mathbf{6}^+$ is assigned to HOMO (t_2) → LUMO (**8**) charge transfer.

Trends of Reduction Potential and CO Stretch. In CH_2Cl_2 solution, **6** (initial scan anodic; peak-to-peak separation, ∼130 mV) displays a quasireversible one-electron cyclic voltammetric response near −0.35 V vs SCE (Table 2) due to the couple of eq 3. Reduction potential data are collected in Table

$$\mathbf{6}^+ + e \rightleftharpoons \mathbf{6} \qquad (3)$$

2. Coulometry of **6** at 0.0 V is attended with the transfer of one electron, quantitatively affording $\mathbf{6}^+$ in solution. The parent radical **6** is fully regenerated upon coulometry of the oxidized solution at −0.6 V.

It was difficult to study the voltammetry of **6** in MeCN due to high oxygen sensitivity. However, this could be done in the case of $\mathbf{6}^+$ (initial scan cathodic) which afforded a nearly reversible (peak-to-peak separation, 60−70 mV) voltammogram representing the couple of eq 3. The $E_{1/2}$ values (Table 2) lie close to those determined using **6** as the electroactive substance.

The $E_{1/2}$ of the $\mathbf{6a}^+$/**6a** couple is ∼50 mV lower than that of the $\mathbf{6b}^+$/**6b** couple. This is consistent with the π-acidity gradation pap < abp. There is a qualitative correlation between the $E_{1/2}$ values and CO stretching frequencies (Table 2) which follow the order **6a** < **6b** and $\mathbf{6a}^+$ < $\mathbf{6b}^+$. Superior π-acidity of abp diminishes the extent of back-bonding to the CO ligand. For a given azo ligand the ν_{CO} values follow the order **6** < $\mathbf{6}^+$, representing a decline of the extent of the net back-bonding to coordinated CO in going from the electron-rich anion radical to the nonradical species. It is believed that back-bonding to CO (and possibly to PPh_3 ligands) plays a significant role in stabilizing the azo anion radical complexes.

Concluding Remarks

The first azo anion radical complexes of osmium have been isolated and characterized in the form of type **6** species. Augmented back-bonding to carbon monoxide and possibly phosphine helps in radical stabilization. The small metal character in the spin-bearing azo-π^* orbital is expressed in EPR anisotropy. The π-acidity order abp > pap is reflected in reduction potential and carbonyl stretching frequency data.

This work taken collectively with those on ruthenium azo anion radical species[5,6] has convincingly demonstrated the value of homolytic M−H cleavage as a rational route for accessing azo anion radical species. We also have here a unique opportunity to observe and contrast two parallel routes: *homolytic* cleavage as above, leading to **6a**, and *heterolytic* Os−Br cleavage, affording **7**. When azo π-acidity is augmented via replacement of pap by abp, the heterolytic route is no longer observable.

The starting materials used so far (**5** and others[5,6]) have a single hydride ligand. Materials with two hydride ligands are under scrutiny; the purpose is to generate and isolate bis(azo anion radical) and (azo)(azo anion radical) complexes. Preliminary results are encouraging.

Experimental Section

General Information. All reactions involving radical syntheses were carried out under an atmosphere of pure and dry nitrogen. The pap and abp ligands were synthesized according to previously published procedures.[19] The starting material, **5**, was prepared by the reported procedure.[11] The chemicals 2-aminopyridine (Aldrich), OsO_4 (Arora-Mathey, India), and NH_4PF_6 (Aldrich) were used as received. Heptane used in the preparation was dried by distillation over Na/benzophenone. The purification of dichloromethane and acetonitrile and the preparation of tetraethylammonium perchlorate (TEAP) for electrochemical work were done as described before.[20]

Physical Measurements. Electronic and IR spectra were recorded with Hitachi 330 and Perkin-Elmer 783 IR spectrophotometers, respectively. For ^1H NMR spectra, a Bruker 300 MHz FT NMR spectrophotometer was used (tetramethylsilane is the internal standard). Magnetic properties were examined using a PAR-155 vibrating sample magnetometer fitted with a Walker Scientific magnet. EPR spectra were recorded on a Varian E-109C spectrometer. Microanalyses (C, H, N) were done by using a Perkin-Elmer 240C elemental analyzer. Electrochemical measurements were performed under nitrogen atmosphere using a PAR 370-4 electrochemistry system as before:[20b] working electrode, SCE; auxiliary electrode, platinum wire; supporting electrolyte, Et_4NClO_4 (0.1 M); scan rate, 50 mV s^{-1}; solution concentration, $\sim 10^{-3}$ M. All potentials reported in this work are uncorrected for junction contribution.

[Os(pap$^{\bullet-}$)(Br)(CO)(PPh_3)$_2$], 6a. To an excess of pap (65 mg, 0.35 mmol) dissolved in dry heptane (30 mL) was added [Os(H)(Br)(CO)(PPh_3)$_3$] (100 mg, 0.09 mmol), and the mixture was heated to reflux for 2 h. The initial orange color gradually changed to dark green. The reaction mixture was then cooled to room temperature and filtered. The residue thus collected was a mixture of green and red components. The green component alone was soluble in benzene and was recovered by evaporating the benzene solution under reduced pressure. It was successively washed with dry acetonitrile and hexane and finally dried in vacuo. Yield 55%. Data for **6a** are as follows. Anal. Calcd (found) for $C_{48}H_{39}BrN_3OOsP_2$: C, 57.31 (57.16); H, 3.92 (3.98); N, 4.18 (4.04).

(18) (a) Goodman, B. A.; Raynor, J. B. *Adv. Inorg. Chem. Radiochem.* **1970**, *13*, 135. (b) Balch, A. L.; Holm, R. H. *J. Am. Chem. Soc.* **1966**, *88*, 5201.

(19) (a) Goswami, S.; Chakravarty, A. R.; Chakravorty, A. *Inorg. Chem.* **1981**, *20*, 2246. (b) Baldwin, A.; Lever, A. B. P.; Parish, R. V. *Inorg. Chem.* **1969**, *8*, 107.

(20) (a) Lahiri, G. K.; Bhattacharya, S.; Ghosh, B. K.; Chakravorty, A. *Inorg. Chem.* **1987**, *26*, 4324. (b) Chandra, S. K.; Basu, P.; Ray, D.; Pal, S.; Chakravorty, A. *Inorg. Chem.* **1990**, *29*, 2423.

Table 2. Electrochemical[a] and IR[b] Data of **6** and **6**$^+$

compd	$E_{1/2}$, V (ΔE_{pc}, mV) L/L$^{\bullet-}$	ν_{CO}, (cm^{-1})	compd	$E_{1/2}$, V (ΔE_{pc}, mV) L/L$^{\bullet-}$	ν_{CO}, (cm^{-1})
6a	−0.38 (120)	1907	**6a**$^+$	−0.40 (70)	1942
6b	−0.33 (140)	1922	**6b**$^+$	−0.34 (70)	1962

[a] **6a**, **6b** in CH_2Cl_2 and **6a**$^+$, **6b**$^+$ in MeCN. [b] In a KBr disk. [c] $\Delta E_p = E_{pa} - E_{pc}$.

UV−vis (C_6H_6) [λ_{max}, nm (ϵ, M^{-1} cm^{-1})]: 610 (2900), 500 (sh, 2700), 450 (sh, 3600), 380 (12 000).

[Os(pap)(H)(CO)(PPh$_3$)$_2$]Br, 7. The red residue left after removal of green **6a** via dissolution in benzene in the above preparation is **7**. It was recrystallized from a dichloromethane−hexane mixture and then dried in a vacuum whereby the solvent of crystallization (vide infra) was lost. Yield 12%. Data for **7** are as follows. Anal. Calcd (found) for $C_{48}H_{40}BrN_3OOsP_2$: C, 57.26 (57.11); H, 4.00 (3.86); N, 4.17 (4.21). UV−vis (CH_2Cl_2) [λ_{max}, nm (ϵ, M^{-1} cm^{-1})]: 515 (3800), 350 (14 500). IR (KBr, cm^{-1}): 1922 (ν_{CO}). Pap/pap$^{\bullet-}$ couple (CH_3CN), $E_{1/2}$, V (ΔE_p, mV): −0.56 (65). ^{1}H NMR ($CDCl_3$, 298 K, ppm from TMS): δ 8.41 (d, J = 8.1, 1H), 8.24 (t, J = 7.5, 1H), 7.5 (m, 2H), 6.80 (t, J = 6.2, 1H), −9.13 (t, J = 22.5, 1H).

[Os(abp$^{\bullet-}$)(Br)(CO)(PPh$_3$)$_2$], 6b. The green crystalline compound was prepared in a way similar to that used for **6a**, except using abp in place of pap. Here there was no red component, and pure **6b** was deposited on cooling the reaction mixture. It was collected by filtration and then washed and dried as in the case of **6a**. Yield 90%. Anal. Calcd (found) for $C_{47}H_{38}BrN_4OOsP_2$: C, 56.07 (55.89); H, 3.80 (3.68); N, 5.56 (5.42). UV−vis (C_6H_6) [λ_{max}, nm (ϵ, M^{-1} cm^{-1})]: 680 (2600), 650 (sh, 2500), 540 (2300), 385 (13 000).

[Os(pap)(Br)(CO)(PPh$_3$)$_2$]PF$_6$, 6a$^+$PF$_6^-$. To a solution of **6a** (50 mg, 0.04 mmol) in dichloromethane (20 mL) was added an acetonitrile (5 mL) solution of NH_4PF_6 (20 mg, 0.12 mmol), and the mixture was magnetically stirred in air until the green color changed to dark brown. The organic solvents were removed under reduced pressure, and the solid was thoroughly washed with water and dried in vacuo. Subsequent chromatographic workup of the dichloromethane solution of the solid on a silica gel column with a 1:4 acetonitrile−benzene mixture as eluent afforded the red-brown complex. Yield 70%.. Anal. Calcd (found) for $C_{48}H_{39}BrF_6N_3OOsP_3$: C, 50.09 (49.84); H, 3.42 (3.27); N, 3.65 (3.71). UV−vis (CH_2Cl_2) [λ_{max}, nm (ϵ, M^{-1} cm^{-1})]: 575 (sh, 2000), 505 (2600), 380 (8400). ^{1}H NMR ($CDCl_3$, 298 K, ppm from TMS): δ 8.78 (d, J = 8.1, 1H), 8.23 (t, J = 7.7, 1H), 7.76 (d, J = 5.7, 1H), 6.90 (t, J = 7.5, 2H), 6.78(t, J = 6.6, 1H), 6.69 (d, J = 8.4, 2H).

[Os(abp)(Br)(CO)(PPh$_3$)$_2$]PF$_6$, 6b$^+$PF$_6^-$. This compound was prepared in a manner similar to that used for **6a**$^+$PF$_6^-$, except for using **6b** as the starting material. Yield 80%. Anal. Calcd (found) for $C_{47}H_{38}BrF_6N_4OOsP_3$: C, 49.01 (49.18); H, 3.33 (3.43); N, 4.86 (4.71). UV−vis (CH_2Cl_2) [λ_{max}, nm (ϵ, M^{-1} cm^{-1})]: 625 (sh, 1350), 535 (2200), 450 (sh, 2900), 365 (8800). ^{1}H NMR ($CDCl_3$, 298 K, ppm from TMS): δ 8.79 (d, J = 7.8, 1H), 8.15 (t, J = 9.0, 1H), 8.14 (d, J = 6.0, 1H), 8.00 (d, J = 5.4, 1H), 7.63 (d, J = 8.1, 1H), 7.52 (t, J = 7.5, 1H), 7.37 (t, J = 5.9, 1H), 7.02 (t, J = 6.6, 1H).

Molecular Orbital Calculation. Extended Hückel calculations and orbital plots were performed using the ICON software package developed by Hoffmann and others.[21,22] The orthogonal coordinate system chosen for the calculations is defined in structures **8** and **9**. The experimental bond distances and angles of **6b** were used in the calculations. The C−H, N−H, and P−H distances were taken as 0.96, 0.90, and 1.42 Å, respectively.

Crystal Structure Determination. Dark green single crystals of **6b** grew directly from the reaction medium in synthesis via careful cooling to room temperature. Single crystals of **7**·CH_2Cl_2 were grown by slow diffusion of hexane into a dichloromethane solution of **7**. The sizes of the crystals of **6b** and **7**·CH_2Cl_2 used for crystallographic measurement were 0.38 × 0.35 × 0.24 and 0.34 × 0.25 × 0.22 mm, respectively. Cell parameters were determined by the least-squares fit of 30 machine-centered reflections (2θ = 15−30°) in each case. Data were collected by the ω-scan technique in the range 1.83° ≤ θ ≤ 25.05° for **6b** and 1.70° ≤ θ ≤ 25.05° for **7**·CH_2Cl_2 on a Siemens R3m/V four-circle diffractometer equipped with a graphite crystal monochromator and Mo Kα (λ = 0.710 73 Å) radiation. Two check reflections measured after every 98 reflections showed no significant intensity reduction in either case. All data were corrected for Lorentz-polarization effects, and an empirical absorption correction was done on the basis of azimuthal scans[23] of six reflections. For **6b**, which was relatively weakly diffracting, 7446 reflections were collected, 6940 were unique, and 3862 satisfying $I > 2.0\sigma(I)$ were used for structure solution. In the case of **7**·CH_2Cl_2 the corresponding numbers are 8353, 7972, and 4960, respectively.

Table 3. Crystallographic Data for **6b** and **7**·CH_2Cl_2

	6b	**7**·CH_2Cl_2
empirical formula	$C_{47}H_{38}BrN_4OOsP_2$	$C_{49}H_{42}BrCl_2N_3OOsP_2$
fw	1006.9	1091.8
cryst syst	monoclinic	monoclinic
space group	$P2_1/c$	$P2_1/n$
a, Å	10.215(4)	15.323(7)
b, Å	17.634(7)	15.201(6)
c, Å	22.473(8)	19.542(7)
β, deg	97.67(3)	92.51(3)
U, Å^3	4012(3)	4547(3)
Z	4	4
T, °C	293	293
λ, Å	0.710 73	0.710 73
D_c, g cm^{-3}	1.670	1.598
μ(Mo Kα), mm^{-1}	4.303	3.918
F(000)	1988	2160
$R1$,[a] $wR2$[b] [$I > 2\sigma(I)$]	0.0866, 0.2012	0.0628, 0.1419
goodness of fit on F^2	1.032	1.056

[a] $R1 = \sum||F_o| - |F_c||/\sum|F_o|$. [b] $wR2 = [\sum w(F_o^2 - F_c^2)^2/\sum w(F_o^2)^2]^{1/2}$.

All calculations for data reduction, structure solution, and refinement were done using the programs of SHELXTL, Version 5.03.[24] Both structures were solved by the Patterson heavy-atom method and were refined by full-matrix least squares on F^2, making non-hydrogen atoms (all in **6b** and all except solvent in **7**·CH_2Cl_2) anisotropic, the hydrogen atoms being added at calculated positions. The hydridic H atom in **7**·CH_2Cl_2 was fixed at a distance of 1.60 Å[25] from the metal; the thermal parameters of the CH_2Cl_2 molecule are high, representing disorder. Significant crystal data are listed in Table 3.

Acknowledgment. Financial support received from the Indian National Science Academy, the Department of Science and Technology, and the Council of Scientific and Industrial Research, New Delhi, is acknowledged. Affiliation with the Jawaharlal Nehru Center for Advanced Scientific Research, Bangalore, is acknowledged.

Supporting Information Available: For **6b** and **7**·CH_2Cl_2, text describing the X-ray structure determination and tables of crystal data, complete atomic coordinates and thermal parameters, bond distances and angles, anisotropic thermal parameters, and hydrogen atom positional and thermal parameters. This material is available free of charge via the Internet at http://pubs.acs.org.

IC9908322

(21) (a) Hoffmann, R. *J. Chem. Phys.* **1963**, *39*, 1397. (b) Ammeter, J. H.; Bürgi, H.-B.; Thibeault, J. C.; Hoffmann, R. *J. Am. Chem. Soc.* **1978**, *100*, 3686.
(22) Maelli, C.; Proserpio, D. M. CACAO, Version 4.0, Firenze, Italy, July 1994. (b) Maelli, C.; Proserpio, D. M. *J. Chem. Educ.* **1990**, *67*, 399.
(23) North, A. C. T.; Philips, D. C.; Mathews, F. S. *Acta Crystallogr.* **1968**, *A24*, 351.
(24) Sheldrick, G. M. *SHELXTL*, Version 5.03; Siemens Analytical Instruments Inc.: Madison, WI, 1994.
(25) Green, M. A.; Huffman, J. C.; Caulton, K. G. *J. Organomet. Chem.* **1983**, *C78*, 243.